

# HelXAS: A low-cost laboratory scale X-ray absorption spectrometer

Ari-Pekka Honkanen,\* Sami Ollikkala, Antti-Jussi Kallio, Merja Blomberg, and Simo Huotari

*Department of Physics, University of Helsinki  
PO Box 64, FI-00014 Helsinki, Finland*

Taru Ahopelto

*Department of Physics, University of Aberdeen  
King's College, Aberdeen,  
AB24 3FX, United Kingdom and  
Department of Physics, University of Helsinki  
PO Box 64, FI-00014 Helsinki, Finland*

(Dated: August 10, 2018)

We present a low-cost laboratory X-ray absorption spectrometer utilizing a conventional X-ray tube source and bent Johann-type crystal monochromators. The instrument is designed for XAS studies in the 5–20 keV range which covers most K edges of  $3d$  transition metals and L edges of  $5d$  transition metals and actinides. The typical energy resolution is around 1–2 eV. Measurements can be performed in transmission, fluorescence, and imaging modes. Due to its simple and modular design, HelXAS can be modified to accommodate additional equipment and complex sample environments required for *e.g.* *in situ* studies. A showcase of various applications is presented.

## I. INTRODUCTION

The idea of laboratory-based X-ray absorption spectroscopy (XAS) instruments is not new but dates back to the advent of X-rays [1, pp. 76–78,97]. With the rise of the extended X-ray fine-structure (EXAFS) technique [2], such instruments were developed in the 1970’s[3, 4] but owing to the advent of dedicated synchrotron light sources and the subsequent proliferation of high brilliance facilities [5, pp. 5–7], the interest toward laboratory instrumentation faded. Thereafter XAS has become a well-established technique for obtaining element-specific information on the local structure and chemical state. But the demand for synchrotron beamtime has increased tremendously, making it a scarce resource. As a consequence, one finds it difficult to access synchrotrons for standard measurements which nevertheless could be crucial for understanding the chemistry and structure of novel materials.

In addition to competition, the use of synchrotrons poses other complications. Especially with complex *in situ* setups and radioactive materials, transporting the relevant equipment and samples to the beamline and back can be a daunting exercise in logistics and bureaucracy. Managing through all this extra-scientific effort, the experimentalists ought to have a strong desire to ensure that also the scientific prerequisites are *par excellence* before arriving at the beamline. A strong cavalcade of pre-characterisation techniques can thus make a difference between a success and a farce.

The aforementioned difficulties, whereas already pointed out by Knapp *et al.* back in 1978, have just recently reignited the spark of interest toward the

laboratory-based X-ray spectrometry [6–11]. In the meanwhile, the manufacturing techniques of bent crystal optics have seen major improvements [12–19] Whereas the instruments in the 1970’s and 1980’s employed mainly cylindrically bent crystal analysers for the monochromatisation of the X-rays, the modern high quality spherically bent analysers have tremendously larger solid angle, increasing the photon flux and the efficiency of the instruments manyfold. This work contributes to the accumulating evidence that the laboratory scale X-ray spectroscopy instruments are not only a viable alternative to synchrotron and free electron lasers but also in certain cases truly complementary to them.

In this manuscript we introduce a low-cost laboratory X-ray absorption spectrometer utilizing a conventional X-ray tube source and bent Johann-type crystal monochromators. Coined HelXAS, the instrument is designed for XANES and EXAFS studies in the 5–20 keV range which covers most K edges of  $3d$  transition metals and L edges of  $5d$  transition metals and actinides. The energy resolution is in the range of 1–5 eV at 10 keV which depends on the analyser crystal and the Bragg angle. Measurements can be performed in transmission and fluorescence detection modes, the latter enabling the study of thick samples or samples on substrate/support. The instrument can be also used for imaging purposes of which a demonstration is given. Due to its simple and modular design, HelXAS can be modified to accommodate additional equipment and complex sample environments required for *e.g.* *in situ* studies. A showcase of various applications is presented.

## II. INSTRUMENT DESIGN

HelXAS is a Johann type spectrometer [20] in which the polychromatic source of X-rays, the spherically bent

\* ari-pekkahonkanen@helsinki.fi

crystal analyser and the detector follow the Rowland circle for proper monochromatisation and focusing of X-rays. The diameter of the Rowland circle is 0.5 m which is dictated by the bending radius of the analyser crystals. The schematic drawing of the main components is shown in Figure 1.

## A. Components

### 1. Source

The X-ray source is a conventional 1.5 kW fine focus X-ray diffraction glass tube with a Ag target. Silver was chosen as the anode material since the Ag K $\alpha$  lines are around 22 keV thus allowing operation in the Bremsstrahlung region up to Mo K edge in the periodic table; therefore it is well suited choice for 3d transition metal K edge and 5d L edge spectroscopy.

The focal spot of the tube is  $0.4 \times 8 \text{ mm}^2$  which at  $6^\circ$  take-off angle transforms to the point source size of  $0.4 \times 0.8 \text{ mm}^2$ , the dimension being perpendicular and parallel to the diffraction plane. The apex angle (or the opening angle) of the X-ray cone is around  $12^\circ$  which illuminates the solid angle covered by the monochromator crystal optimally.

### 2. Monochromator

For monochromatisation and focusing the polychromatic X-rays HelXAS uses so-called strip-bent spherically bent crystal analysers (SBCAs) provided by ESRF Crystal Analyser Laboratory [17]. In our case the SBCAs have the the bending radius of 0.5 m and the surface diameter of 100 mm. Spherical bending causes strain fields in the monochromator which affect its energy resolution [21–24]. The surfaces are cut into 15 mm wide strips to mitigate the effect. In the designed operational range, the typical energy resolution of the analyser is  $\gtrsim 1 \text{ eV}$ .

In principle, position-sensitive detectors can also be used to improve the energy resolution thanks to dispersion compensation both in bent [25] and so-called diced analyser crystals [26, 27].

### 3. Detectors and counting electronics

HelXAS is designed to be flexibly used with detectors for transmission, fluorescence, and imaging modes. The simultaneous data acquisition with multiple detectors is possible.

Currently for the transmission mode measurements a standard NaI scintillator detector with a single channel analyser is employed. The dead time of the scintillator setup is  $\tau = 2.8 \mu\text{s}$ . For the fluorescence mode we utilize an Amptek XR-100T CdTe semiconductor detector in

conjunction with a multichannel analyser. The active area of the detector is  $7 \text{ mm}^2$ .

In addition to the more traditional detectors, HelXAS has a readily available imaging option utilizing Advacam Modupix detector. The detector is build around the silicon Timepix chip[28] consisting of  $256 \times 256$  array of  $55 \times 55 \mu\text{m}^2$  pixels.

### 4. Motors and Movement

The Rowland circle geometry is followed by three motorized linear translation stages, one motorized goniometer, a passive rotation stage with a telescopic steering bar as presented in Figure 2.

The Bragg angle  $\theta_B$  of the monochromator crystal adjusted with the Huber goniometer. The smallest step size is  $0.000125^\circ$  or  $2.18 \mu\text{rad}$ . The analyser-goniometer complex rests on a linear stage which adjusts the source-monochromator distance  $\rho$  based on set  $\theta_B$  according to  $\rho = R_b \sin \theta_B$ , where  $R_b$  is the bending radius of the SBCA (or the diameter of the Rowland circle). In addition to the motorized degrees of freedom, the analyser stage has two manual actuators to adjust the tilt and the height of the analyser crystal.

The distance of the detector from the monochromator is adjusted with a motorized linear stage which is installed on the freely rotating stage. The telescopic steering bar keeps the detector directed at the monochromator. The rotating stage is installed on another linear translation stage which follows the monochromatized beam. Motors and data acquisition is run on SPEC version 6 by Certified Scientific Software.

### 5. Sample Changer

HelXAS is equipped with a sample changer which allows automatisation of batch measurements. For transmission measurements, we use a stepper motor controlled circular plate design depicted in Figure 3 positioned in front of the tube. The sample plates are easily changeable which allows the accommodation of special sample requirements *e.g.* anaerobic environment. The sample changer can be used also at the detector side for radiation sensitive transmission samples and in fluorescence measurements.

### 6. Enclosure

The instrument is enclosed in a cabinet pictured in Figure 4. The user safety is ensured by specifically positioned lead shielding to absorb the directed beams, whereas the aluminium walls of the enclosure are itself thick enough to block any stray scattering and fluorescent radiation. The windows of the glass doors are lead glass. The dimensions of the enclosure are  $200 \times 100 \times 80 \text{ cm}^3$ .

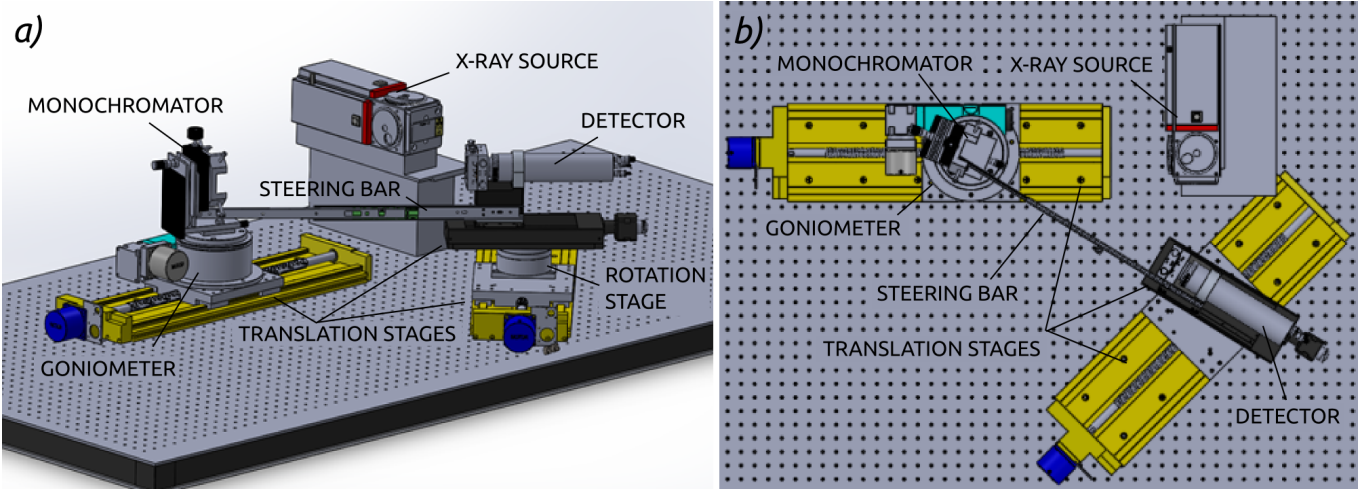


FIG. 1: Schematic drawing of the essential parts of the instrument from a) side and b) top

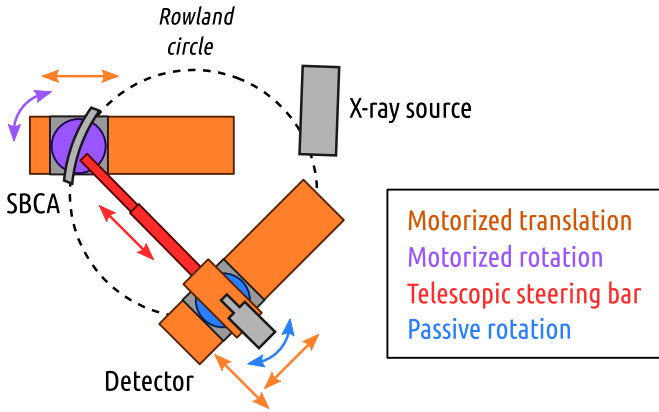


FIG. 2: Motor configuration and degrees of freedom

## B. Operation

The main use of HelXAS is the determination of the absorption coefficient  $\mu_x$  as the function of photon energy either directly from the attenuation of the beam transmitted through the sample or indirectly from the fluorescence yield.

The transmission configuration is presented in Figure 5. For transmission measurements the sample can be positioned either in front of the tube or in front of the detector. The advantage with the former is the stability of the beam footprint; owing to the spherical aberration, the vertical and horizontal focal lengths differ considerably at the detector side as a function of the Bragg angle. Therefore the footprint of the beam through the sample varies during the scan which might cause artefacts to the spectrum if the optical thickness of the sample is not uniform. In front of the tube the beam footprint is stable but since the beam is polychromatic, the radiation dose rate is considerably larger which may harm more sensitive samples.

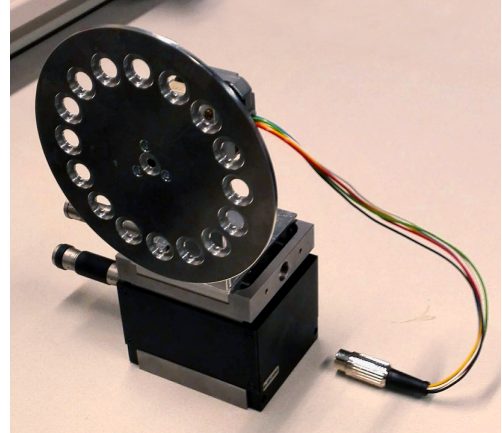


FIG. 3: Sample changer with 15 sample positions + 1 direct beam aperture



FIG. 4: Instrument enclosure

Since modern X-ray tubes and their power sources are highly stable, the measurements of the direct and transmitted beams can be conducted separately using the same detector without the need for additional beam monitor. In addition, since  $\mu_x$  depends on the beam intensities in a highly non-linear manner, the background levels owing

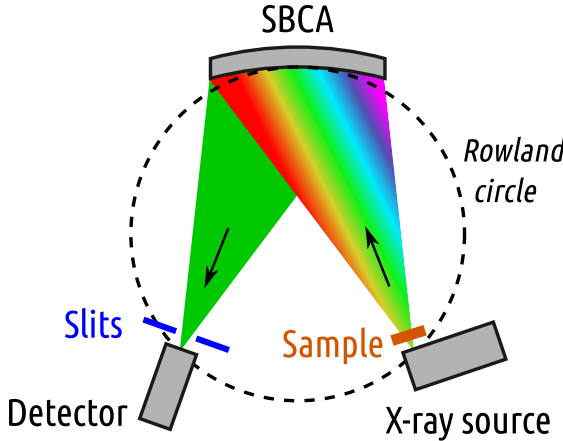


FIG. 5: Direct absorption measurement in transmission mode. Alternatively, the sample can be placed in front of the detector.

air scattering and fluorescence of components needs to be determined and subtracted from the signals proper. This is done by offsetting the detector from the beam focus and repeating the scan. To obtain an accurate estimate of the background at the focal spot, the offset measurement is performed on both sides of the focus. A low-order polynomial is fitted to the mean of the background signals and the fit is subtracted from the recorded signals. Therefore the absorption coefficient is obtained from the Beer-Lambert law by

$$\mu x = -\ln \frac{I - y_{bg}}{I_0 - y_{0,bg}}, \quad (1)$$

where  $I_0$  and  $I$  are the direct and the transmitted beam intensities and  $y_{0,bg}$  and  $y_{bg}$  are the smoothing polynomials of their background signals, respectively.

The fluorescence mode configuration is presented in Figure 6. As with the transmission measurements the signal from the sample and the reference signal are usually measured separately. For the reference signal for element with atomic number  $Z$ , one may use fluorescence from a  $Z - 1$  foil. Alternatively, if the absorption of the sample and the possible substrate is low, one could measure the reference signal from the transmitted beam with the scintillator. However, since the detector and thus the beam spot moves on the sample, this may introduce geometrical contributions to the spectrum which do not normalize out properly.

For optically thin sample ( $\mu x \ll 1$ ), the absorption coefficient is directly proportional to the fluorescence signal:

$$\mu x \propto I_f/I_0 \quad (2)$$

where  $I_f$  is the fluorescence signal from the sample and  $I_0$  is the reference signal. Fluorescence mode can be used also for thick samples but in that case the data has to be corrected for the self-absorption.

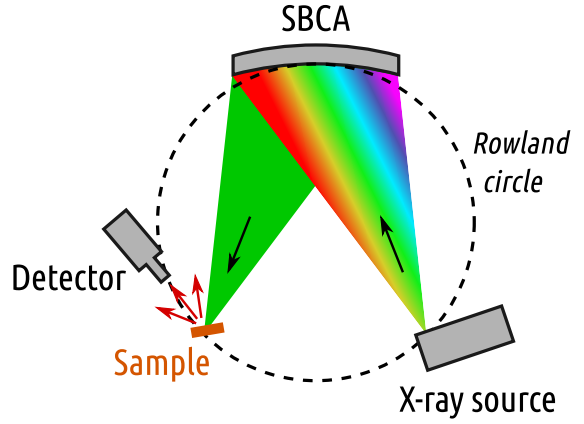


FIG. 6: Indirect absorption measurement in fluorescence mode.

The Python implementations of the data extraction routines are available at <https://github.com/aripekka/helxas>.

### III. USE CASES

#### A. XANES

The most standard application of the instrument is to measure X-ray absorption near-edge structure, or XANES, in transmission mode. As a benchmark, we measured the XANES of 10  $\mu\text{m}$  thick cobalt foil using Si(533) monochromator. The X-ray tube acceleration voltage was 20 kV and the current 2 mA. Fairly low tube power was used to in order avoid the saturation of the scintillator detector with the direct beam.

Average direct beam count rate normalized to the tube current was 20 kcps/mA·s of which the background contribution was 0.6–1 kcps/mA·s, the level decreasing with increasing photon energy. The below the Co K edge, the count rate of the beam transmitted through the foil was 13 kcps/mA·s. Above the Co K edge the count rate was 0.9 kcps/mA·s. The background contributions were 0.2–0.3 kcps/mA·s, the level decreasing with the increasing photon energy. The direct beam was scanned 18 times and the foil 29 times, each scan consisting of 301 energy point and counting time 5 seconds per point. The background measurements were done in the same manner for the transmitted and the direct beam, totalling 4 scans. Total counting time not including the motor movement was thus 21.3 hours.

We note that such a long total counting time is overextensive as the resulting statistical accuracy is as small as 0.25 %. Making the background scans shorter by the factor of 4, one obtains already with 7 scans of both the sample and the direct beam better than 0.5 % accuracy in 6.3 hours. Even with 2 scans each, we get better than 1.0 % accuracy in 2.1 hours. One could go even beyond that; if the scintillator was replaced with a high count

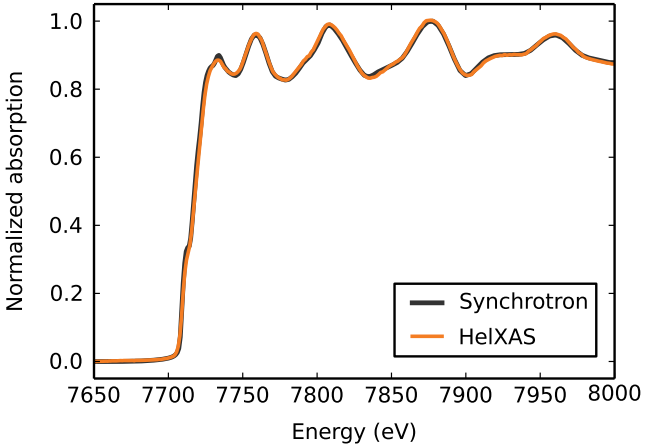


FIG. 7: Normalized K edge absorption spectrum of cobalt foil compared with the synchrotron reference measured at NSLS X11B [29].

rate detector like a silicon drift diode, which would not saturate even for the maximum tube current of 40 mA, we could obtain 0.3 % statistical accuracy in less than 1.5 hours.

The result is presented together with literature data obtained at synchrotron[29] in Figure 7. The measured spectrum corresponds well to the reference over all 300 eV range. Slight deviations, especially at the main edge, are most likely owing to the fact, that the energy resolution of HelXAS, estimated to be order of 2 eV, is not quite as high as the one of a synchrotron beam line but more than sufficient for most applications.

### B. EXAFS: long k-range measurement

In the normal configuration the lowest attainable Bragg angle is around  $67^\circ$  which is limited by the range of the larger translation stage of the detector (see Fig. 2). However, the range can be considerably extended by performing the measurement in parts for different translation stage positions. This makes it possible to measure extended X-ray absorption fine-structure (EXAFS) up to 1000 eV or more above the absorption edge.

The EXAFS acquisition was demonstrated with a 5  $\mu\text{m}$  thick nickel foil using a Si(551) monochromator. The spectrum was measured over two Bragg angle ranges:  $81\text{--}67^\circ$  and  $69\text{--}57^\circ$ . The overlap of the ranges was to assure the proper stitching of the parts. The X-ray tube voltage and the current for the ranges were 10 kV/5 mA and 10 kV/10 mA, respectively. Untypically low acceleration voltage was used to avoid the excitation of W  $\text{L}_3$  electrons at 10.2 keV and thus the presence of W  $\text{La}_{1,2}$  lines which overlap with the Ni K edge. The presence of tungsten in the tube is most likely owing to the evaporation of the filament.

The current-normalised count rates of the direct beam

were 0.6–4 kcps/mA·s and the background rates 0.1–0.3 kcps/mA·s, both decreasing toward the higher photon energies. The count rates of the transmitted beam were 3 kcps/mA·s below the Ni K edge and 0.3–0.9 kcps/mA·s above. The background rates were 0.2–0.05 kcps/mA·s. The direct and the transmitted beams in the low-energy part were measured 15 and 30 times, respectively, with 401 points per scan and 5 seconds counting time per point. In the high-energy part the numbers of scans were 10 and 21, for the direct and the transmitted beams respectively, with 301 points and 10 seconds per point. The total counting time including the background scans was 53.2 hours.

The measured absorption spectrum is presented in Figure 8 a. With the two-part measurement, the EXAFS region can be obtained up to 1400 eV above the edge, which corresponds almost  $20 \text{ 1}/\text{\AA}$  in  $k$ -space, as seen in Figure 8 b. The EXAFS signal and its Fourier transform compare well to the synchrotron literature reference[29] in quality (Figures 8 b and c).

### C. Detection in fluorescence mode

The fluorescence mode was tested with two samples. The first one was a 10  $\mu\text{m}$  thick cobalt metal foil which was scanned 65 times, 301 points per scan. The counting time was 10 s/point, totalling 54.3 hours. The total intensity of Co  $\text{K}\alpha$  fluorescence signal above the edge was 60–70 counts/s of which the background contribution was 30 counts/s. In order to normalize the signal, the fluorescence of an iron foil was measured over the same energy grid. The Fe foil was measured 54 times, 5 s/point, totalling 22.6 hours. The count rate was 50–60 photons/second. The tube voltage was 20 kV and the current was 10 mA in both cases.

For normalisation the Fe signal was smoothed with a polynomial fit. The measured fluorescence was corrected for the self-absorption using Athena [29]. For correction, the incidence angle value was set to  $90^\circ$  and outgoing value was chosen to be  $15^\circ$ . The measured and corrected fluorescence signals are presented together with Co absorption spectrum measured in transmission mode in Figure 9. The self-absorption corrected fluorescence signal is found to follow the transmission spectrum as expected.

The second sample measured was a 100 nm thick  $\text{Co}_3\text{O}_4$  film[30] grown on a silicon substrate using atomic layer deposition[31, 32]. The sample was scanned 4 times, 301 points per scan. The counting time per point was 50 seconds, totalling 16.7 hours of counting time. The count rate above the edge was 10–15 photons/second, of which the background contribution was 8.5 photons/s. The tube voltage and current were 20 kV and 40 mA respectively. In order to increase the statistics, the data was binned in the groups of three data points in the data analysis phase. The measured spectrum together with the reference oxide spectra measured in transmission are presented in Fig. 10. The data follows clearly the  $\text{Co}_3\text{O}_4$

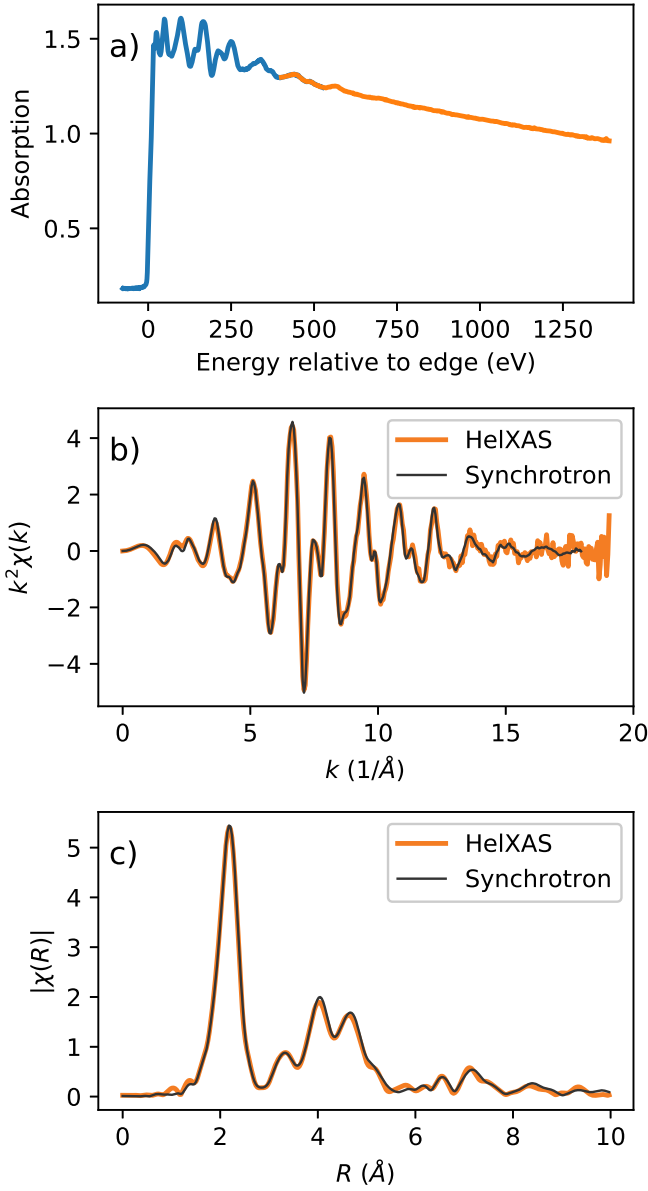


FIG. 8: EXAFS spectrum of nickel foil at Ni K edge. a) Raw absorption spectrum measured in two parts b) Extracted EXAFS oscillations c) Fourier transform of the EXAFS oscillations. The synchrotron reference was measured at APS 13ID [29].

reference, allowing us to discriminate between the different species of cobalt oxides with high confidence.

To our knowledge this is the first time when X-ray absorption spectrum is measured *via* fluorescence using a laboratory scale instrument. An observant reader has noticed, though, that currently the signal quality is far from optimal. The main challenge in the fluorescence mode is the poor signal-to-noise ratio which substantially prolongs the measurement times. The high background signal originates from the fluorescence excited by radiation scattered by the air and components of the instruments.

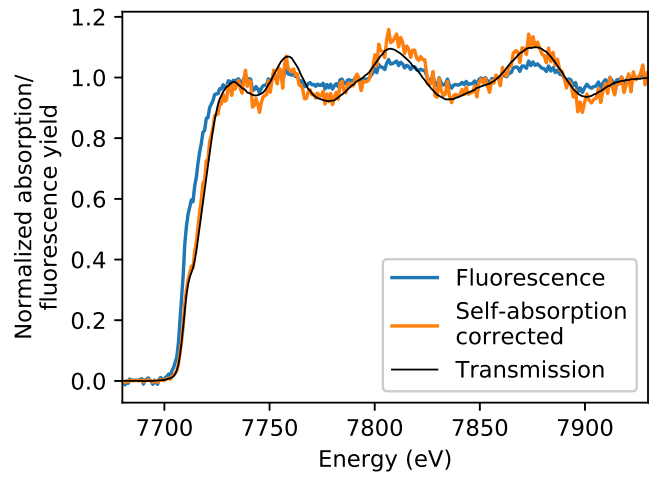


FIG. 9: Cobalt K $\alpha$  fluorescence yield spectrum measured in fluorescence mode from Co foil (blue), the same signal after self-absorption correction (orange) and the absorption spectrum measured in transmission mode (black).

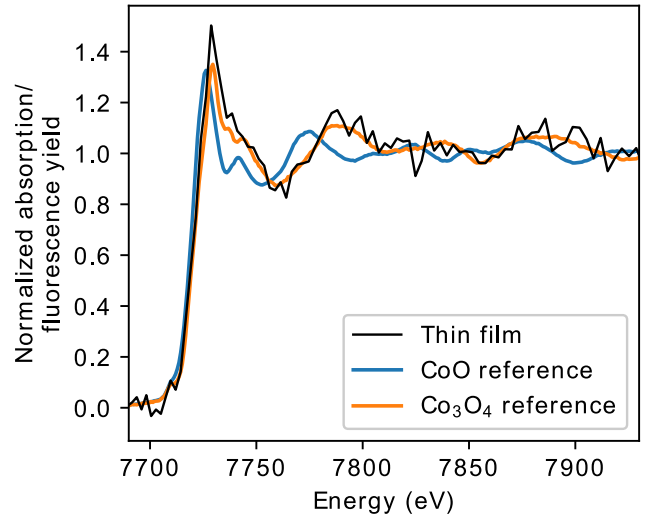


FIG. 10: Cobalt K edge spectrum measured in fluorescence mode from 100 nm Co<sub>3</sub>O<sub>4</sub> thin film grown with atomic layer deposition (gray). In comparison, the reference powders measured in transmission mode are presented in blue and orange.

Its contribution could be minimized with a helium filled box, radiation shielding and slitting, and optimization of the detector distance and the orientation with respect to the sample.

#### D. Imaging

The combination of a monochromatic beam and a position-sensitive detector allows us to utilise absorption

edge subtraction as a contrast mechanism in transmission imaging thus allowing the element sensitive mapping of the sample. The idea of the absorption edge subtraction imaging is to take absorption images slightly above and below the absorption edge of interest. Except for the element in question, the absorption coefficients vary slowly over a small energy range giving a strong contrast to the parts of the sample containing the element of interest in the difference image [33].

The test sample was a steel washer filled with potato starch embedded with small amounts of NiO, NiO<sub>2</sub>, and Co<sub>3</sub>O<sub>4</sub> powders (Fig. 11a). The inner diameter of the washer was 11 mm and the thickness was 1 mm. The sample was attached in front of the detector and the detector was placed into the cone of the monochromatic beam out of the focus in a way that the detector chip was fully illuminated. Two images were taken of the sample, one below and another above the Co K-edge. Another two images were taken without the sample (*i.e.* the flat field images) at the corresponding photon energies. Due to the low noise of the detector, the dark field images without the beam could be omitted. The transmission images obtained by taking the logarithm of the flat field normalized frames are presented Figures 11b and 11c. The distribution of cobalt is then extracted by subtraction of the below and above edge images. The result is presented in Fig. (11d).

This proof-of-concept study indicates that the element-sensitive imaging is a viability with a Johann type laboratory spectrometer. With further development, the method can be potentially used to study not only the distribution of elements in the sample but also their chemical state by pinpointing the position of the absorption edge. The presented method can provide valuable information in laboratory scale, for example, in *in situ* battery and *in vivo* biological studies. In addition, the absorption edge subtraction imaging can be readily combined with computed tomography to obtain 3D reconstruction with element contrast of the sample.

#### IV. APPLICATIONS

In this section we present various real-life projects for which HelXAS has been used. The purpose of the showcase is to highlight the advantages of having a laboratory scale instrument readily available.

The development and synthesis of new electrochemical materials for energy devices is an active and rapidly advancing field of materials science. X-ray absorption spectroscopy would be a valuable tool in understanding the chemical composition and oxidation states of the newly synthesised sample but suffers from the scarcity of synchrotron beamtime available for the materials characterisation, and lengthy and uncertain beamtime application process. Such standard measurements are an ideal use case for our instrument which we demonstrated recently in cases of mesoporous MnCo<sub>2</sub>O<sub>4</sub> and LaMnO<sub>3+δ</sub> elec-

trocatalysts [34, 35].

X-ray absorption spectroscopy is also suitable for non-invasive biochemical studies, for example, to investigate the binding and activity of metallic ions in proteins and peptides [36, 37] or metabolism of toxic elements in plants and animals [38, 39]. Using HelXAS, we have investigated the bioaccumulation of selenium in *Pseudomonas* T5-6-I bacteria. The bacteria cultivated in SeO<sub>3</sub><sup>-2</sup> rich solution were freeze-dried and Se K edge was measured from them in the dormant state. The preliminary results presented in Figure 12 show that the selenium is accumulated by *Pseudomonas* as Se(0) which is consistent with the earlier studies [40]. The in-depth analysis is under preparation [41].

The actinides are very important group of elements with regards nuclear energy production and waste management but owing to their radioactive nature, their chemistry is relatively poorly known. XAS is widely used method for studying their chemistry and composition but its usage is severely limited by the lack of suitable beamlines. It was recently demonstrated that laboratory scale spectrometers are a viable option for actinide research by measuring the uranium L<sub>3</sub> edges from several oxides of uranium [42]. Owing to the compact size, similar instruments could be integrated with the handling equipment of radioactive materials which allows the XAS studies of highly active materials in a safe manner.

A unique application of the laboratory scale XAS is the possibility to run extremely long *in situ* chemical reaction studies. We have studied [43] the chemistry of Co nanoparticles used to catalyse the formation of long hydrocarbon chains from hydrogen and carbon monoxide in Fischer-Tropsch synthesis. The longest *in situ* runs have lasted over 200 hours which excludes the possibility of conducting the same experiment at synchrotrons. In such experiments the laboratory based instruments in fact complementary to the synchrotron studies.

#### V. CONCLUSIONS

With the access to the synchrotron becoming increasingly scarce, the interest toward laboratory scale X-ray spectroscopy instruments has grown recently. In this work we have introduced our Johann type X-ray absorption spectrometer coined HelXAS which is a versatile and low-cost setup capable of measuring absorption spectra of most 3d K and 5d L edges in both transmission and fluorescence modes. In addition, the use of position sensitive detector amends the instrument with imaging capabilities. The various real-life applications presented show that such instruments have a huge potential in alleviating the need for synchrotron and free electron laser beamtime and sometimes even complement them.

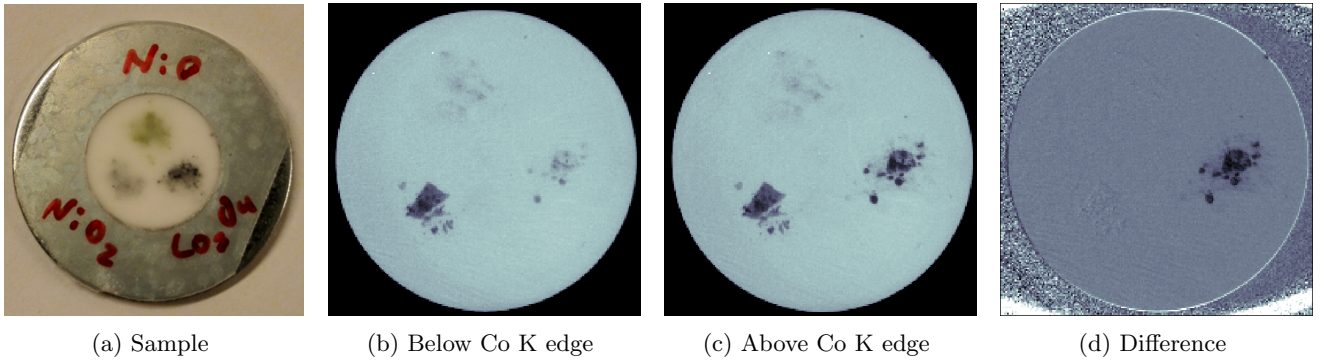


FIG. 11: Absorption edge subtraction imaging using a position-sensitive detector. The images of the sample (powders embedded in potato starch) are taken at photon energies above and below the absorption edge allowing the element-sensitive imaging.

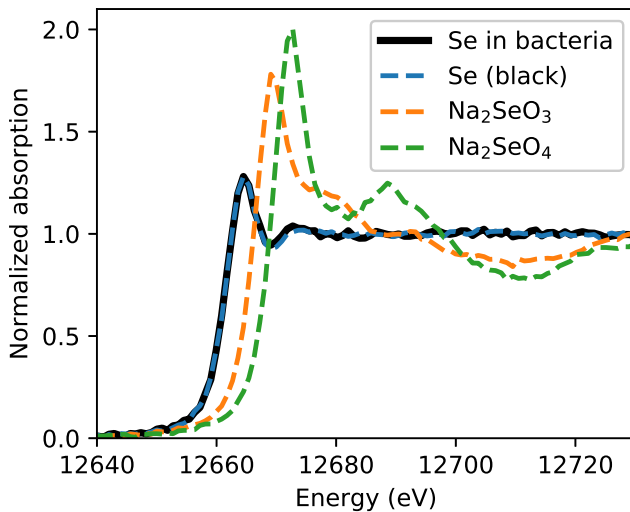


FIG. 12: Se K edge of accumulated selenium in *Pseudomonas* bacteria compared with reference spectra

### Acknowledgements

The authors want to thank Gerald T. Seidler for insightful discussions regarding the instrument design, Tomi Iivonen for providing the cobalt oxide thin film sample and Papa Sene for the CAD drawings of the instrument.

- 
- [1] L. V. Azároff, *Elements of X-ray Crystallography* (McGraw-Hill Book Company, 1968) international Student Edition.
  - [2] D. E. Sayers, E. A. Stern, and F. W. Lytle, Physical Review Letters **27**, 1204 (1971), doi:10.1103/physrevlett.27.1204.
  - [3] G. S. Knapp, H. Chen, and T. E. Klippert, Review of Scientific Instruments **49**, 1658 (1978), doi:10.1063/1.1135340.
  - [4] A. A. Bahgat and K. D. Gupta, Review of Scientific Instruments **50**, 1020 (1979), doi:10.1063/1.1135970.
  - [5] H. Winick, *Synchrotron Radiation Sources — A Primer* (WORLD SCIENTIFIC, 1995) doi:10.1142/2444.
  - [6] Y. N. Yuryev, H.-J. Lee, H.-M. Park, Y.-K. Cho, M.-K. Lee, and K. J. Pogrebitsky, Review of Scientific Instruments **78**, 025108 (2007), doi:10.1063/1.2669591.
  - [7] M. Szlachetko, M. Berset, J.-C. Dousse, J. Hoszowska, and J. Szlachetko, Review of Scientific Instruments **84**, 093104 (2013), doi:10.1063/1.4821621.
  - [8] G. T. Seidler, D. R. Mortensen, A. J. Remesnik, J. I. Pacold, N. A. Ball, N. Barry, M. Styczinski, and O. R. Hoidn, Review of Scientific Instruments **85**, 113906 (2014), doi:10.1063/1.4901599.
  - [9] C. Schlesiger, L. Anklaam, H. Stiel, W. Malzer, and B. Kanngießer, Journal of Analytical Atomic Spectrometry **30**, 1080 (2015), doi:10.1039/c4ja00303a.
  - [10] Z. Németh, J. Szlachetko, É. G. Bajnóczki, and G. Vankó, Review of Scientific Instruments **87**, 103105 (2016), doi:10.1063/1.4964098.
  - [11] L. Miaja-Avila, G. C. O’Neil, Y. I. Joe, B. K. Alpert, N. H. Damrauer, W. B. Doriese, S. M. Fatur, J. W. Fowler, G. C. Hilton, R. Jimenez, C. D. Reintsema, D. R. Schmidt, K. L. Silverman, D. S. Swetz, H. Tat-

- suno, and J. N. Ullom, *Physical Review X* **6** (2016), doi:10.1103/physrevx.6.031047.
- [12] U. Bergmann and S. P. Cramer, in *Crystal and Multilayer Optics*, edited by A. T. Macrander, A. K. Freund, T. Ishikawa, and D. M. Mills (SPIE, 1998) doi:10.1117/12.332507.
- [13] E. Collart, A. Shukla, F. Gélibart, M. Morand, C. Malgrange, N. Bardou, A. Madouri, and J.-L. Pelouard, *Journal of Synchrotron Radiation* **12**, 473 (2005), doi:10.1107/s090904950501472x.
- [14] R. Verbeni, M. Kocsis, S. Huotari, M. Krisch, G. Monaco, F. Sette, and G. Vankó, *Journal of Physics and Chemistry of Solids* **66**, 2299 (2005), doi:10.1016/j.jpcs.2005.09.079.
- [15] H. Yavaş, E. E. Alp, H. Sinn, A. Alatas, A. H. Said, Y. Shvyd'ko, T. Toellner, R. Khachatryan, S. J. Billinge, M. Z. Hasan, and W. Sturhahn, *Nuclear Instruments and Methods in Physics Research Section A: Accelerators, Spectrometers, Detectors and Associated Equipment* **582**, 149 (2007), doi:10.1016/j.nima.2007.08.095.
- [16] R. Verbeni, T. Pylkkänen, S. Huotari, L. Simonelli, G. Vankó, K. Martel, C. Henriet, and G. Monaco, *Journal of Synchrotron Radiation* **16**, 469 (2009), doi:10.1107/s090904950901886x.
- [17] M. Rovezzi, C. Lapras, A. Manceau, P. Glatzel, and R. Verbeni, *Review of Scientific Instruments* **18**, 013108 (2017), doi:10.1063/1.4974100.
- [18] Saint-Gobain Crystals, <http://www.crystals.saint-gobain.com/> (Accessed 8th Aug. 2018).
- [19] XRS TECH LLC., <http://xrstech.com/> (Accessed 8th Aug. 2018).
- [20] H. H. Johann, *Zeitschrift für Physik* **69**, 185 (1931), doi:10.1007/BF01798121.
- [21] S. Takagi, *Acta Crystallographica* **15**, 1311 (1962), doi:10.1107/s0365110x62003473.
- [22] D. Taupin, *Bulletin de la Société Française de Minéralogie et de Cristallographie* **87**, 469 (1964).
- [23] S. Takagi, *Journal of the Physical Society of Japan* **26**, 1239 (1969), doi:10.1143/jpsj.26.1239.
- [24] A.-P. Honkanen, R. Verbeni, L. Simonelli, M. M. Sala, G. Monaco, and S. Huotari, *Journal of Synchrotron Radiation* **21**, 104 (2014), doi:10.1107/s160057751302242x.
- [25] A.-P. Honkanen, R. Verbeni, L. Simonelli, M. M. Sala, A. Al-Zein, M. Krisch, G. Monaco, and S. Huotari, *Journal of Synchrotron Radiation* **21**, 762 (2014), doi:10.1107/s1600577514011163.
- [26] S. Huotari, G. Vankó, F. Albergamo, C. Ponchut, H. Graafsma, C. Henriet, R. Verbeni, and G. Monaco, *Journal of Synchrotron Radiation* **12**, 467 (2005), doi:10.1107/s0909049505010630.
- [27] S. Huotari, F. Albergamo, G. Vankó, R. Verbeni, and G. Monaco, *Review of Scientific Instruments* **77**, 053102 (2006), doi:10.1063/1.2198805.
- [28] X. Llopis, R. Ballabriga, M. Campbell, L. Tlustos, and W. Wong, *Nuclear Instruments and Methods in Physics Research Section A: Accelerators, Spectrometers, Detectors and Associated Equipment* **581**, 485 (2007), 10.1016/j.nima.2007.08.079.
- [29] B. Ravel and M. Newville, *Journal of Synchrotron Radiation* **12**, 537 (2005), doi:10.1107/S0909049505012719.
- [30] J. Kim, T. Iivonen, J. Hääläinen, M. Kemell, K. Meinander, K. Mizohata, L. Wang, J. Räisänen, R. Beranek, M. Leskelä, and A. Devi, *Chemistry of Materials* **29**, 5796 (2017), 10.1021/acs.chemmater.6b05346.
- [31] T. Suntola, *Materials Science Reports* **4**, 261 (1989), doi:10.1016/s0920-2307(89)80006-4.
- [32] M. Leskelä and M. Ritala, *Thin Solid Films* **409**, 138 (2002), doi:10.1016/s0040-6090(02)00117-7.
- [33] R. Lewis, *Physics in Medicine and Biology* **42**, 1213 (1997), 10.1088/0031-9155/42/7/001.
- [34] W. Wang, L. Kuai, W. Cao, M. Huttula, S. Ollikkala, T. Ahopelto, A.-P. Honkanen, S. Huotari, M. Yu, and B. Geng, *Angewandte Chemie* **129**, 15173 (2017), doi:10.1002/ange.201708765.
- [35] L. Kuai, E. Kan, W. Cao, M. Huttula, S. Ollikkala, T. Ahopelto, A.-P. Honkanen, S. Huotari, W. Wang, and B. Geng, *Nano Energy* **43**, 81 (2018), doi:10.1016/j.nanoen.2017.11.018.
- [36] F. A. Lima, T. J. Penfold, R. M. van der Veen, M. Reinhard, R. Abela, I. Tavernelli, U. Rothlisberger, M. Benfatto, C. J. Milne, and M. Chergui, *Phys. Chem. Chem. Phys.* **16**, 1617 (2014), doi:10.1039/c3cp53683a.
- [37] B. Alies, A. Conte-Daban, S. Sayen, F. Collin, I. Kieffer, E. Guillou, P. Faller, and C. Hureau, *Inorganic Chemistry* **55**, 10499 (2016), doi:10.1021/acs.inorgchem.6b01733.
- [38] E. Lombi, K. G. Scheckel, J. Pallon, A. M. Carey, Y. G. Zhu, and A. A. Meharg, *New Phytologist* **184**, 193 (2009), doi:10.1111/j.1469-8137.2009.02912.x.
- [39] S. Misra, D. Peak, and S. Niogi, *Metalomics* **2**, 710 (2010), doi:10.1039/c0mt00008f.
- [40] M. Lusa, , J. Knuutinen, and M. B. and, *AIMS Microbiology* **3**, 798 (2017), doi:10.3934/microbiol.2017.4.798.
- [41] M. Lusa et al., In preparation.
- [42] R. Bès, T. Ahopelto, A.-P. Honkanen, S. Huotari, G. Leinders, J. Pakarinen, and K. Kvashnina, *Journal of Nuclear Materials* **507**, 50 (2018), doi:10.1016/j.jnucmat.2018.04.034.
- [43] J. G. Moya-Cancino, A.-P. Honkanen, F. Meirer, F. M. F. de Groot, S. Huotari, and B. M. Weckhuysen, “In-situ x-ray absorption near edge structure spectroscopy of a solid catalyst using a laboratory-scale set-up,” In preparation.